Optics Letters

High-beam-quality, watt-level, widely tunable, mid-infrared OP-GaAs optical parametric oscillator

Q. Fu, L. Xu,* S. Liang, P. C. Shardlow, D. P. Shepherd, S.-U. Alam, and D. J. Richardson

Optoelectronics Research Centre, University of Southampton, Southampton, SO17 1BJ, UK
**Corresponding author: l.xu@soton.ac.uk*

Received 19 February 2019; revised 25 March 2019; accepted 26 March 2019; posted 26 March 2019 (Doc. ID 360322); published 23 May 2019

We demonstrate near-diffraction-limited performance from a mid-infrared, idler-resonant, fiber-laser-pumped, widely tunable, picosecond optical parametric oscillator (OPO) based on orientation-patterned gallium arsenide (OP-GaAs). The OP-GaAs OPO is synchronously pumped by a picosecond Tm:fiber master–oscillator-power-amplifier system. An OPO tuning range of 4394–6102 nm (idler) and 2997–3661 nm (signal) is achieved, with maximum average powers of 1.18 (idler, 5580 nm) and 0.51 W (signal, 3136 nm). The idler beam has M^2 values of 1.06 (x-direction) by 1.03 (y-direction).

https://doi.org/10.1364/OL.44.002744

Mid-infrared (mid-IR) (2 to 20 μm) tunable ultrafast pulses are of importance for applications in the area of stand-off chemical sensing and imaging, because this wavelength range corresponds to the fundamental rotational-vibrational transitions of numerous molecules [1–6]. Mid-IR sources with wide tuning capability, a narrow spectral linewidth, high average power, good beam quality, and a high repetition rate, therefore, are in demand for such spectroscopic applications. Wide tuning allows access to the detection of different molecules, whereas narrow linewidths are important for spectral resolution. High power improves the signal-to-noise ratio and a high repetition rate increases the data processing speed. Furthermore, good beam quality is crucial for remote sensing and imaging, as it allows a longer measurement distance. Apart from spectroscopic applications, good beam qualities are also of benefit in material processing and surgery, which require strong focusing [7,8]. High beam quality is also good for optical fiber integrated systems such as power delivery and nonlinear optics [9].

Quantum cascade lasers, lead-salt diode lasers, and interband cascade lasers can provide mid-IR and even far-infrared outputs, but can only produce relatively low peak power and a limited tuning range from single devices [1,10,11]. Optical parametric devices, taking advantage of the development of quasi-phase matching (QPM) crystals such as periodically poled lithium niobate, orientation-patterned gallium arsenide (OP-GaAs), and orientation-patterned gallium phosphide (OP-GaP), have also received much attention as mid-IR sources [1,12]. In particular, OP-GaAs has a broad transparency window of 0.9–17 μm, a large nonlinear coefficient of 94 pm/V (d_{14}), and good thermal and mechanical properties [13], but it has to be pumped by lasers with wavelengths of >1.7 μm due to two-photon absorption at shorter wavelengths [12]. 2 μm thulium-doped fiber (Tm:fiber) lasers, therefore, are a good candidate for pumping OP-GaAs-based mid-IR parametric devices [14–19]. In 2017, our group reported a Tm:fiber-laser pumped OP-GaAs optical parametric generator (OPG) and optical parametric amplifier (OPA). The OP-GaAs OPG had a broad tuning range (2550–2940 nm for the signal and 5800–8300 nm for the idler), but with a high threshold and limited output power (maximum 260 mW) [14]. The OP-GaAs OPA had a higher output power of 1.07 (signal) and 0.26 W (idler), but its relatively narrow wavelength tunability was limited by the seed laser. In our later work, a new configuration of Tm:fiber-laser pumped cascaded OP-GaAs OPG-OPA was developed having a tuning capability covering the whole phase-matched spectrum provided by the OP-GaAs crystal; however, the output beam qualities were relatively poor with $M^2 \sim 2.2$ (signal) and ~3.4 (idler) [15]. In contrast to OPGs and OPAs, optical parametric oscillators (OPOs) can potentially generate high output power, a broad tuning range, and good beam quality simultaneously. However, typical signal-resonant OPOs provide poor long-wavelength output beam quality, while idler-resonant OPOs have rarely been studied and, so far, have only been demonstrated at relatively short wavelengths in the mid-IR [20–23].

Here we report an idler-resonant, mid-IR, fiber-laser-pumped, widely tunable, picosecond, OP-GaAs OPO with near-diffraction-limited idler beam quality and watt-level average output power. The OP-GaAs OPO was synchronously pumped by a 2007 nm Tm:fiber master-oscillator-power-amplifier (MOPA) system generating ~100 ps duration pulses at a 100 MHz repetition rate. A tuning range of 4394–6102 nm (idler) and 2997–3661 nm (signal) was demonstrated by changing the temperature and using different patterning periods of the OP-GaAs crystal. A maximum average power of 1.18 (idler, 5580 nm) and 0.51 W (signal, 3136 nm) was obtained. The slope efficiencies were 19.6% and 8.6% for the idler and signal, respectively. The maximum peak powers of the idler and signal were calculated to be more than 118 (idler) and 51 W

(signal). The idler beam quality was measured to be $M_x^2 = 1.06$ and $M_y^2 = 1.03$. To the best of our knowledge, these results represent the first report of an idler-resonant synchronously fiber-laser-pumped OP-GaAs OPO with near-diffraction-limited beam qualities at idler wavelengths.

The OPO pump system (Tm:fiber MOPA) is shown in Fig. 1(a), and switched the OP-GaAs OPO configuration is shown in Fig. 1(b). The pump source was based on a 2007 nm gain-laser diode (GSLD) seed laser, operating at a repetition rate of 100 MHz with an average power of ~100 μW, followed by four Tm:fiber amplifier stages. Two fiber Bragg gratings [Fig. 1(a)], with reflective bandwidths of 0.2 and 0.5 nm, combined with two circulators, were used after the first and second amplifier stages, respectively, to filter and suppress the longitudinal side modes of the GSLD, as well as to remove excess amplified spontaneous emission. Note that the final linewidth of the MOPA was governed by these two FBGs, rather than the seed laser diode. The first and second pre-amplifier stages were core-pumped by erbium/ytterbium co-doped fiber lasers at 1564 nm with pump powers of 0.8 and 3 W, respectively. A 16 m long Tm:fiber (OFS TmDF200) and a 2 m-long home-made Tm:fiber (8.5 μm core, 100 μm cladding, NA = 0.2) were employed as gain fibers to increase the output power to 39 and 170 mW for the first and second amplifier stages. Due to the spectral filtering by the FBGs and the losses of optical elements such as circulators (3 dB), only 2 and 44 mW of power were launched into the second and third pre-amplifier stages, respectively. The third pre-amplifier used a 4 m long Tm:fiber (Nufern, PM-TDF-10P/130-HE) cladding-pumped by a 792 nm laser diode and provided an output power of 200 mW at the operational pump power of 1.4 W. Isolators [not shown in Fig. 1(a)] were placed after the GSLD and each amplifier stage in order to avoid back reflections. The power amplifier consisted of a 2.5 m long polarization-maintaining 25 μm core Tm:fiber [Fig. 1(a), Nufern, PLMA-TDF-25P/400-HE] pumped by two 791 nm laser diodes with a total pump power of 43 W, providing an output signal power of 15 W. The output beam was linearly polarized and had a spatial beam quality of $M^2 = 1.5$. An 8 deg angled endcap was spliced to the end of the Tm:fiber to enlarge the beam diameter at the air-glass interface to avoid potential optical damage, as well as to inhibit backward reflection of light coupled back into the amplifier. The output spectrum did not suffer any significant nonlinear broadening in the amplifier fibers, and the 3 dB bandwidth was measured to be 0.2 nm (0.5 cm^{-1}). This is well within the calculated OP-GaAs pump acceptance bandwidth (~1.3 nm) based on Sellmeier data of GaAs [24]. Because of the many optical elements between the pump system [Fig. 1(a)] and the OPO cavity [Fig. 1(b)], the maximum available pump power immediately before the crystal for the OPO was 11 W. Two half-wave plates (HWP1, 2), combined with a polarizing beam splitter were used to control both the pump power and the rotation of the linear polarization incident onto the crystal. To realize maximal quasi-phase matching in OP-GaAs, the polarization direction was aligned along the [111] crystallographic axis. The OP-GaAs crystal (BAE Systems) had periods of 57–65 μm, with a step of 2 μm. Each channel had dimensions of 20 mm length (along $[1\bar{1}0]$), 1 mm thickness (along [001]), and 5 mm width (along [110]). The OP-GaAs was mounted in an oven to allow temperature tuning from 20°C to 200°C. Both end facets of the OP-GaAs were anti-reflection (AR) coated at the pump ($R < 1\%$), idler ($R < 1.5\%$), and signal ($R < 5\%$) wavelengths. The OPO cavity consisted of two plane-concave dielectric-coated mirrors (M1, M2, Fig. 1, radius of curvature = 250 mm), and four plane-plane gold-coated mirrors. The plane-concave mirrors were AR coated at the pump wavelength ($R < 2\%$) and high-reflection (HR) coated at idler wavelengths ($R > 99.5\%$). The plane-concave mirror coatings were not specifically designed for the signal wavelengths, which led to a variation in reflectivity of 1–70% over the entire signal wavelength range. The total optical cavity length was set to 3 m to match the pump repetition rate of 100 MHz, so as to achieve a synchronously pumped ring resonator. The OP-GaAs crystal was placed in the middle of two plane-concave mirrors, which were separated by 276 mm. The cavity mode of the idler beam was calculated to have a beam waist of 90–110 μm inside the crystal, depending on the idler wavelength. In order to match the cavity modes; the pump beam was focused into the OP-GaAs by a coated CaF_2 lens ($f = 250$ mm) with a beam waist of 100 μm (x direction) and 80 μm (y direction) ($1/e^2$ radius of intensity) due to the slightly elliptical shaped pump beam caused by the angled output facet. Thus, the pump and idler beam were both spatially and temporally overlapped inside the crystal. The idler output was extracted using a coated calcium fluoride beam splitter (BS, Fig. 1, BSW511R, Thorlabs) with a reflectivity of ~24–35% over the idler wavelength range. With the pump polarization set to the [111] crystallographic axis, the output idler is expected to have the same polarization direction in order to obtain the maximum gain [25]. The idler power was measured after a long-pass filter [LPF, Fig. 1(b)], which had a short-wavelength cutoff at 4.5 μm. The signal beam was partially extracted from the cavity through M2 and with the aid of two dichroic mirrors [DM1, DM2, Fig. 1(b)] to separate it from the residual pump light.

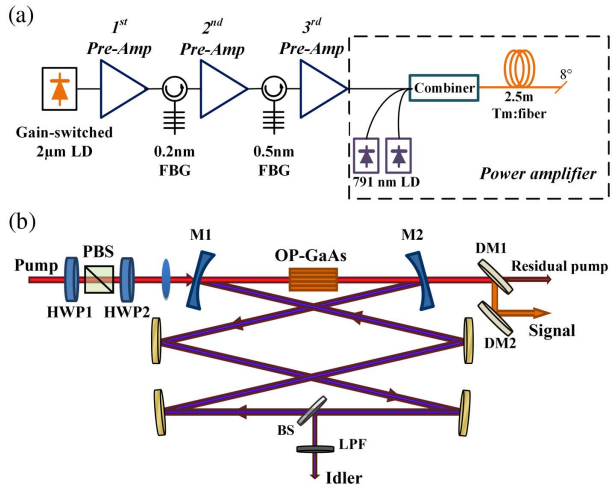

Fig. 1. (a) Thulium-doped fiber MOPA system. LD, laser diode; FBG, fiber Bragg grating; Tm:fiber, thulium-doped fiber. (b) OP-GaAs OPO experimental setup. HWP, half-wave plate; PBS, polarizing beam splitter; M1, M2, mirror 1,2; DM, dichroic mirror; LPF, long-pass filter.

At a pump power of 11 W, a maximum idler average power of 1.18 W was obtained from the 59 μm OP-GaAs working period at an oven temperature of 80°C. Under the same operating conditions, slightly lower maximum idler output powers of 1.1 and 0.8 W were obtained from the 57 and 61 μm OP-GaAs

working periods, respectively. We attribute this to the associated changes in the cavity mode and the lower idler quantum efficiency over the different wavelengths. Figure 2 shows the idler and signal output powers working with 59 μm OP-GaAs period at a temperature of 80°C with the idler and signal wavelengths of 5580 and 3136 nm. An oscillation threshold of 5 W was observed corresponding to a pump intensity of ~2.5 MW/cm^2 (theoretical threshold intensity ~1 MW/cm^2 [26]). An idler slope efficiency of 19.6% and a maximum optical-to-optical conversion efficiency of 10.7% were observed without any roll-off phenomenon, meaning the OPO output power was primarily limited by the available pump power. The signal output from DM2 was measured and is plotted in Fig. 2 (left) with a maximum output power and slope efficiency of 0.51 W and 8.6%, respectively. Taking into consideration all of the output mirror losses (76%), the generated signal power from the crystal was calculated to be ~1.96 W. Unfortunately, we were unable to directly measure the duration of the signal and idler pulses due to a lack of suitable characterization equipment; however, the signal and idler pulses are generally expected to be shorter than the pump pulses in the OPA due to nonlinear gain narrowing effects [27]. Consequently, we infer that the peak powers of the generated idler and signal pulses are at least 118 and 51 W, respectively [i.e., higher than the values calculated assuming that the signal and idler pulses have the same pulse duration as the pump (100 ps)]. The operation of the Tm:fiber MOPA system and OPO was reasonably stable over time. We measured a <3% drift in the pump power and ~8% in the OPO output power over a period of about 30 min. The larger drift on the OPO output was due to drift in the OPO cavity alignment, and this was readily corrected by mechanical retuning of the cavity mirrors.

Tunability was studied by using different OP-GaAs grating periods and oven temperatures. The idler and signal wavelengths could be tuned from 4394–6102 nm (idler) and 2997–3661 nm (signal), as shown in Fig. 3. The signal and idler spectra were characterized by an optical spectrum analyzer (Bristol Instruments 771 series, 0.1 nm resolution) and a monochromator (Bentham TMc300, 0.3 nm resolution), respectively. A typical spectral linewidth of 14 (4.5 cm^{-1}) and 1 nm (1.0 cm^{-1})

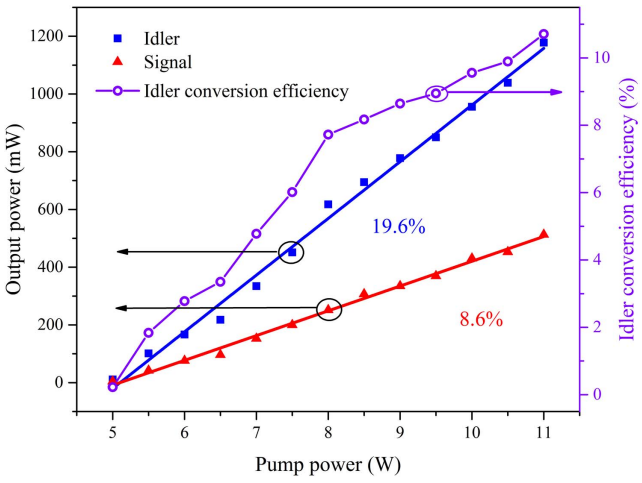

Fig. 2. (Left): idler (5580 nm) and signal (3136 nm) output power as a function of the pump power from the OPO. The squares and triangles are measured data points, and the solid lines are linear fits. (Right): idler power conversion efficiency versus the pump power. The solid line is purely to guide the eye.

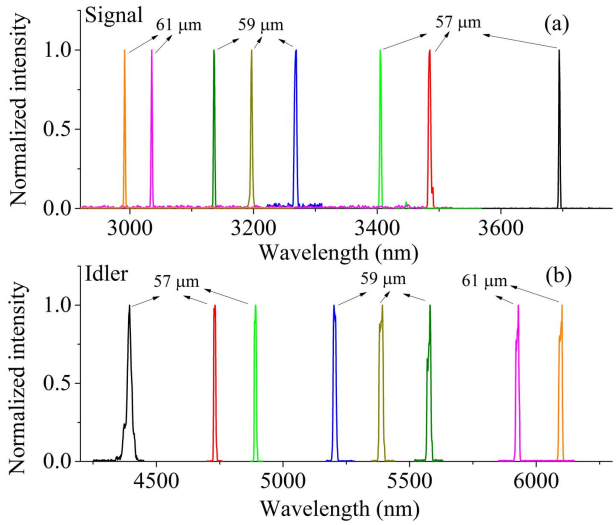

Fig. 3. Measured OPO (a) signal and (b) idler spectra and their corresponding working crystal periods.

were observed for the generated idler and signal, respectively. The OPO was operated with three different OP-GaAs periods of 57, 59, and 61 μm, but did not work with periods of 63 and 65 μm. With OP-GaAs periods of 63 and 65 μm, the OPO idler wavelength should be able to reach ~7 μm, with corresponding signal wavelengths as short as ~2.8 μm. We believe it was not possible to reach a threshold for these wavelengths due to the higher losses associated with the crystal AR coatings ($R = 90\%$ at 7 μm), the plane-concave mirror coatings ($R = 88\%$ at 7 μm), and the BS coating (1% absorption at 7 μm). We have selected to design this particular OPO to work at around 6 μm as a potential source for supercontinuum generation in chalcogenide optical fibers. This application also requires a good beam quality as is addressed in the next section.

The OPO signal [Fig. 4(a)] and idler [Fig. 4(b)] beam quality was characterized by using a pyroelectric scanning profiler (NanoScan, Photon). At the maximum output power, the idler beam quality was measured to be $M_x^2 = 1.06$ and $M_y^2 = 1.03$ due to the spatial control imposed by the idler-resonant OPO

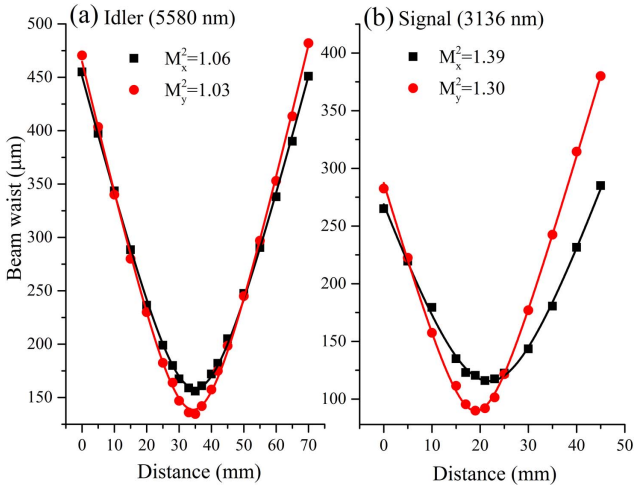

Fig. 4. OP-GaAs OPO (a) idler (5580 nm) and (b) signal (3136 nm) beam qualities.

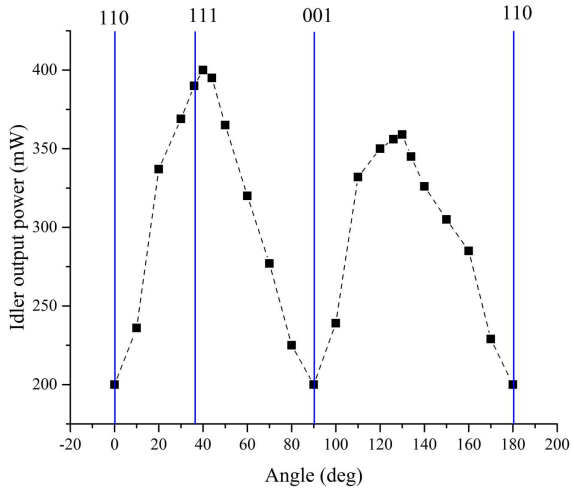

Fig. 5. Idler average output power versus the angle of pump polarization. The blue line is the OP-GaAs crystal axis.

cavity. Also at the maximum output, the signal beam quality was characterized to be slightly worse than that of the idler, with a value of $M_x^2 = 1.39$ and $M_y^2 = 1.30$ which, however, is marginally better than the pump beam. The slight elliptical beam shape followed that of the pump beam shape, as expected.

The influence of the pump polarization on the nonlinear frequency conversion in the OP-GaAs was also investigated. As the coated BS was polarization sensitive, we replaced the coated BS (Fig. 1) with an uncoated calcium fluoride wedge (WW51050, Thorlabs). In order to reduce the influence of different amplitude transmission coefficients for *s* and *p* polarizations, the angle of incidence of the light on the uncoated calcium fluoride wedge was limited to ∼10°. The generated idler output power against the angle of the input pump polarization is plotted in Fig. 5. According to theoretical models, the effective nonlinear coefficient has a maximum value when the pump polarization is aligned to the [111] direction (35° to the [110]) direction [24]. We observed a global maximum idler output power in close agreement with the theoretical prediction, as shown in Fig. 5. The minor disagreement may be caused by measurement error and/or thermal- or stress-induced birefringence [19].)

In summary, an idler-resonant, fiber-laser-pumped, widely tunable, mid-IR, picosecond, fiber-laser-pumped OPO based on OP-GaAs has been demonstrated. The OPO tuning range is 4394–6102 nm (idler) and 2997–3661 nm (signal). A maximum average power of 1.18 (idler, 5580 nm) and 0.51 W (signal, 3136 nm) was obtained. The highest peak powers of idler and signal were calculated to be more than 118 and 51 W, respectively. The signal beam quality was characterized to be $M_x^2 = 1.39$ and $M_y^2 = 1.30$, whereas the idler beam quality was much better with $M_x^2 = 1.06$ and $M_y^2 = 1.03$. The combination of broadband tunability in the mid-IR, watt-level average power, and high spatial coherence makes this picosecond OPO a good option for spectroscopy applications and for further nonlinear frequency conversion such as supercontinuum generation.

Funding. Engineering and Physical Sciences Research Council (EPSRC) (EP/I02798X/1, EP/P030181/1); AirGuide Photonics Programme; RIRPLD.

Acknowledgment. The authors thank Dr. Peter Schunemann from BAE Systems for growing the OP-GaAs crystals and are grateful to the China Scholarship Council for supporting Qiang Fu's work. The data can be found in Dataset 1, Ref. [28].

REFERENCES

1. I. T. Sorokina and K. L. Vodopyanov, *Solid-State Mid-Infrared Laser Sources* (Springer, 2003).
2. Z. Zhang, R. J. Clewes, C. R. Howle, and D. T. Reid, Opt. Lett. **39**, 6005 (2014).
3. M. W. Sigrist, J. Adv. Res. **6**, 529 (2015).
4. L. Maidment, Z. Zhang, C. R. Howle, and D. T. Reid, Opt. Lett. **41**, 2266 (2016).
5. R. Ostendorf, L. Butschek, S. Hugger, F. Fuchs, Q. Yang, J. Jarvis, C. Schilling, M. Rattunde, A. Merten, J. Grahmann, D. Boskovic, T. Tybussek, K. Rieblinger, and J. Wagner, Photonics **3**, 28 (2016).
6. M. Vainio and L. Halonen, Phys. Chem. Chem. Phys. **18**, 4266 (2016).
7. A. Godard, C. R. Physique **8**, 1100 (2007).
8. V. A. Serebryakov, É. V. Boĭko, N. N. Petrishchev, and A. V. Yan, J. Opt. Technol. **77**, 6 (2010).
9. A. Sincore, J. Cook, F. Tan, A. El Halawany, A. Riggins, S. McDaniel, G. Cook, D. V. Martyshkin, V. V. Fedorov, S. B. Mirov, L. Shah, A. F. Abouraddy, M. C. Richardson, and K. L. Schepler, Opt. Express **26**, 7313 (2018).
10. I. Sergachev, R. Maulini, A. Bismuto, S. Blaser, T. Gresch, and A. Muller, Opt. Express **24**, 19063 (2016).
11. A. Spott, E. J. Stanton, A. Torres, M. L. Davenport, C. L. Canedy, I. Vurgaftman, M. Kim, C. S. Kim, C. D. Merritt, W. W. Bewley, J. R. Meyer, and J. E. Bowers, Optica **5**, 996 (2018).
12. P. G. Schunemann, in *Advanced Solid State Lasers (ASSL)*, OSA Technical Digest (online) (Optical Society of America, 2015), paper AM2A.2.
13. T. Skauli, K. L. Vodopyanov, T. J. Pinguet, A. Schober, O. Levi, L. A. Eyres, M. M. Fejer, J. S. Harris, B. Gerard, L. Becouarn, E. Lallier, and G. Arisholm, Opt. Lett. **27**, 628 (2002).
14. L. Xu, Q. Fu, S. Liang, D. P. Shepherd, D. J. Richardson, and S.-U. Alam, Opt. Lett. **42**, 4036 (2017).
15. Q. Fu, L. Xu, S. Liang, D. P. Shepherd, D. J. Richardson, and S.-U. Alam, IEEE J. Sel. Top. Quantum Electron. **24**, 1 (2018).
16. K. F. Lee, C. Mohr, J. Jiang, P. G. Schunemann, K. L. Vodopyanov, and M. E. Fermann, Opt. Express **23**, 26596 (2015).
17. O. H. Heckl, B. J. Bjork, G. Winkler, P. Bryan Changala, B. Spaun, G. Porat, T. Q. Bui, K. F. Lee, J. Jiang, M. E. Fermann, P. G. Schunemann, and J. Ye, Opt. Lett. **41**, 5405 (2016).
18. V. O. Smolski, H. Yang, S. D. Gorelov, P. G. Schunemann, and K. L. Vodopyanov, Opt. Lett. **41**, 1388 (2016).
19. J. Wueppen, S. Nyga, B. Jungbluth, and D. Hoffmann, Opt. Lett. **41**, 4225 (2016).
20. L. Xu, J. S. Feehan, L. Shen, A. C. Peacock, D. P. Shepherd, D. J. Richardson, and J. H. V. Price, Appl. Phys. B **117**, 987 (2014).
21. Y. He, F. Chen, D. Yu, K. Zhang, Q. Pan, and J. Sun, Infrared Phys. Technol. **95**, 12 (2018).
22. F. Bai, Q. Wang, Z. Liu, X. Zhang, W. Lan, X. Tao, and Y. Sun, Appl. Phys. B **112**, 83 (2013).
23. K. A. Tillman, D. T. Reid, D. Artigas, and T. Y. Jiang, J. Opt. Soc. Am. B **21**, 1551 (2004).
24. T. Skauli, P. S. Kuo, K. L. Vodopyanov, T. J. Pinguet, O. Levi, L. A. Eyres, J. S. Harris, M. M. Fejer, B. Gerard, L. Becouarn, and E. Lallier, J. Appl. Phys. **94**, 6447 (2003).
25. K. L. Vodopyanov, O. Levi, P. S. Kuo, T. J. Pinguet, J. S. Harris, M. M. Fejer, B. Gerard, L. Becouarn, and E. Lallier, Opt. Lett. **29**, 1912 (2004).
26. D. C. Hanna, M. V. O'Connor, M. A. Watson, and D. P. Shepherd, J. Phys. D **34**, 2440 (2001).
27. L. Xu, H.-Y. Chan, S.-U. Alam, D. J. Richardson, and D. P. Shepherd, Opt. Express **23**, 12613 (2015).
28. https://doi.org/10.5258/SOTON/D0898.